



## A Numerical Study of the Effect of Aspect Ratio on Heat Transfer in an Annular Flow Through a 270-Degree Curved Pipe

Mohammad Hossein Seraji, Hasan Khaleghi\*

Department of Mechanical Engineering, Tarbiat Modares University, Tehran, Iran

Received: 3 February 2019, Revised: 11 March 2019, Accepted: 13 March 2019

© University of Tehran 2019

### Abstract

In the present paper, a three-dimensional annular developing incompressible laminar flow through a 270-degree curved pipe is numerically simulated. The dimensionless governing equations of continuity, momentums, and energy are driven in toroidal coordinates. The governing equations are discretized by projection algorithm using the forward difference for time and central difference for space. A three-dimensional computer code together with a grid generation program is developed in toroidal coordinates by which the present results were obtained. There is a non-uniform heat source  $q''=Be^{A\theta}$  in the solid core and the outer wall is assumed to be adiabatic. Considering the effect of Reynolds number on thermo-hydraulic properties such as the formation of secondary flow and axial velocity, it is possible to increase heat transfer using a non-uniform heat flux instead of the uniform one. The numerical results indicated that the average Nusselt number is increased by imposing a non-uniform heat flux compared with the uniform one assuming that both have the same average flux values. Also, the results indicated heat transfer increases as the aspect ratio is reduced.

### Keywords:

Annular Flow,  
Curved Pipe,  
Non-Uniform Heat  
Source,  
Projection Algorithm,  
Toroidal Coordinates,

### Introduction

The flow through the curved tube is widely visible in both industry and nature such as blood flow in arteries, lubrication systems and especially in heat exchangers due to an increase of heat transfer and reduction of size. Owing to these extensive applications, it is important to identify the hydrodynamic and thermal characteristics of this flow. For the first time, this flow was studied analytically by Dean [1]. His analytical solution is just valid for very low curvature ratio with the assumption of fully developed throughout the pipe. To examine the effect of curvature on the flow field, he introduced the dimensionless parameter of the Dean number,  $De = 2a/R(w_{avg}a/\nu)^2$ , where  $a$  is the radius of the pipe,  $R$  radius of curvature,  $w_{avg}$  the mean axial velocity and  $\nu$  the kinematic viscosity. To increase the accuracy of the solution, Robertson and Muller [2] avoided Dean's simplifying assumption, in which the radius of the pipe had been ignored by the curvature radius, and accommodated momentum equations in its full form. Also, analytical correlations of the streamlines, in the pipe with a slight curvature ratio, are obtained

\* Corresponding author

E-mail: khaleghi@modares.ac.ir (H. Khaleghi)

by Kapur, et al. [3]. As mentioned, the analytical solution can just be used for very low curvature ratio of about 0.01, but for higher curvature ratio, a numerical solution is needed.

The hydrodynamic characteristics of the flow through 270-degree curved pipe are studied numerically by Choi and Park [4]. Petrakis and Karahalios [5] determined the maximum axial velocity and its location in laminar flow using a numerical solution. They also examined a more extensive range of aspect ratios for a 180-degree curved pipe [6]. The results, for aspect ratio about 1000, indicated that the behavior of flow was very similar to flow through a curved pipe without a solid core. In both works, firstly, flows are studied hydrodynamically, without heat transfer, secondly, flow is assumed to be fully developed throughout the pipe. Karahalios [7] studied the formation of secondary flow. Park [8] simulated numerically flow through a 90-degree and 180-degree curved pipe with the assumption of fully developed flow throughout the pipe. He considered horizontal inlet flow and vertical outlet flow through 90-degree pipe. Secondary streamlines for incompressible laminar flow through 180-degree curved pipe are obtained numerically by Gaun and Martonen [9]. Tarbel and Samuels [10] have studied a Newtonian fluid in laminar flow through a 180-degree curved pipe. They had simplified momentum equations, with the assumption of fully-developed throughout the pipe, based on vorticity and streamline functions. The location of vortex formation and decay are determined by Pantokratoras [11] using the straight pipes before and after the inlet and outlet of a 90-degree curved pipe. The boundary layer development of flow through the curved pipe is studied numerically by Riley [12]. Kamal Hasan [13] has investigated thermo-hydraulic characteristics of flow through a 135-degree curved pipe. The inlet velocity is considered to be parabolic and the wall temperature is assumed to be constant. Dutta and Nandi [14] have studied numerically the effect of Reynolds number on the flow through a 90-degree pipe. The entrance length of flow through the curved pipe has reported by Austin and Seader [15]. Also, the transitional Reynolds number is determined by Siggers and Waters [16]. One of the main purposes of applying curved pipes in heat exchangers is the increase in heat transfer. In the present paper, a non-uniform heat source is imposed at the solid core of the pipe. Owing to the physical structure of the secondary flow, the non-uniform function for the heat source is chosen to increase the amount of heat transfer compared with the uniform one. With this in mind, the function of heat flux is accommodated as  $q'' = Be^A\theta$  where  $q''$  is the heat flux,  $\theta$  the angular coordinate and both A and B are constant so that both of the uniform and non-uniform heat sources consume the same amount of energy. Eventually, computer code in Fortran language is developed for 3D thermo-hydraulic simulation of the flow through 270-degree annulus curved pipe (Fig.1).

## Governing Equations

The best coordinates for fluid flow through the torus pipe are the toroidal coordinates. So the governing equation including continuity, full Navier-Stokes and energy equations are derived in the toroidal coordinates system. Based on the following non-dimensional parameters, the governing equations are written in the dimensionless form.

$$\begin{aligned}
 u &= \frac{u^*}{w_{avg}} & v &= \frac{v^*}{w_{avg}} & w &= \frac{w^*}{w_{avg}} & r &= \frac{r^*}{D_h} & R_c &= \frac{R_c^*}{D_h} & t &= \frac{t^*}{D_h/w_{avg}} \\
 p &= \frac{p^*}{\rho w_{avg}^2} & Re &= \frac{w_{avg} D_h}{\nu} & N &= \frac{r_o}{r_i} & T &= \frac{T^* - T_{in}^*}{q''/D_h k}
 \end{aligned} \tag{1}$$

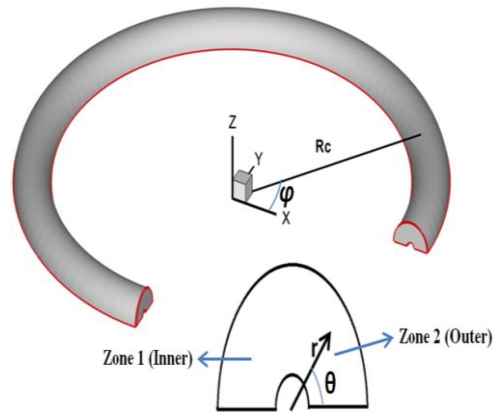


**Fig. 1.** Schematic 270-degree annulus curved pipe

where,  $R_c$  is the dimensionless curvature radius,  $D_h$  the hydraulic diameter,  $N$  the aspect ratio,  $u$ ,  $v$ ,  $w$  dimensionless velocity components in the  $r$ ,  $\theta$  and  $\varphi$  directions, respectively.  $w_{avg}$  is the mean axial velocity,  $r$  the radius,  $\nu$  the kinematic viscosity,  $t$  the dimensionless time,  $q''$  the heat flux of source and  $Re$  the Reynolds number. The variables with superscript \* are representative of its corresponding dimensionless parameters. So, the non-dimensional governing equations including the continuity, full Navier-Stokes in the  $r$ ,  $\theta$  and  $\varphi$  direction as well as energy equation are expressed as:

$$\frac{\partial}{\partial r}(ur\eta) + \frac{\partial}{\partial \theta}(v\eta) + \frac{\partial}{\partial \varphi}(rw) = 0 \quad (2)$$

$$\begin{aligned} \frac{\partial u}{\partial t} + \frac{1}{r\eta} \left[ \frac{\partial}{\partial r}(r\eta u^2) + \frac{\partial}{\partial \theta}(\eta v u) + \frac{\partial}{\partial \varphi}(r u w) - r w^2 \cos(\theta) - \eta v^2 \right] = \\ - \frac{\partial p}{\partial r} + \frac{1}{Re} \left\{ \frac{1}{r\eta} \left[ \frac{\partial}{\partial r}(r\eta \frac{\partial u}{\partial r}) + \frac{\partial}{\partial \theta}(\frac{\eta}{r} \frac{\partial u}{\partial \theta}) + \frac{\partial}{\partial \varphi}(\frac{r}{\eta} \frac{\partial u}{\partial \varphi}) \right] - \frac{2}{r^2} \left( \frac{\partial v}{\partial \theta} \right) \right. \\ \left. - \frac{1}{r^2} u + \frac{\sin(\theta)}{r\eta} v - \frac{\cos(\theta)}{\eta^2} \left[ 2 \frac{\partial w}{\partial \varphi} + u \cos(\theta) - v \sin(\theta) \right] \right\} \end{aligned} \quad (3)$$

$$\begin{aligned} \frac{\partial v}{\partial t} + \frac{1}{r\eta} \left[ \frac{\partial}{\partial r}(r\eta u v) + \frac{\partial}{\partial \theta}(\eta v^2) + \frac{\partial}{\partial \varphi}(r v w) + \eta v w + r w^2 \sin(\theta) \right] = \\ - \frac{1}{r} \frac{\partial p}{\partial \theta} + \frac{1}{Re} \left\{ \frac{1}{r\eta} \left[ \frac{\partial}{\partial r}(r\eta \frac{\partial v}{\partial r}) + \frac{\partial}{\partial \theta}(\frac{\eta}{r} \frac{\partial v}{\partial \theta}) + \frac{\partial}{\partial \varphi}(\frac{r}{\eta} \frac{\partial v}{\partial \varphi}) \right] - \frac{2}{r^2} \left( \frac{\partial u}{\partial \theta} \right) - \frac{1}{r^2} v \right. \\ \left. + \frac{\sin(\theta)}{\eta^2} \left[ 2 \frac{\partial w}{\partial \varphi} + u \cos(\theta) - v \sin(\theta) \right] - \frac{\sin(\theta)}{r\eta} u \right\} \end{aligned} \quad (4)$$

$$\begin{aligned} \frac{\partial w}{\partial t} + \frac{1}{r\eta} \left[ \frac{\partial}{\partial r}(r\eta u w) + \frac{\partial}{\partial \theta}(\eta v w) + \frac{\partial}{\partial \varphi}(r w^2) + r u w \cos(\theta) - r v w \sin(\theta) \right] = \\ - \frac{1}{\eta} \frac{\partial p}{\partial \varphi} + \frac{1}{Re} \left\{ \frac{1}{r\eta} \left[ \frac{\partial}{\partial r}(r\eta \frac{\partial w}{\partial r}) + \frac{\partial}{\partial \theta}(\eta \frac{\partial w}{\partial \theta}) + \frac{\partial}{\partial \varphi}(\frac{r}{\eta} \frac{\partial w}{\partial \varphi}) \right] + \frac{2 \cos(\theta)}{\eta^2} \left( \frac{\partial u}{\partial \varphi} \right) \right. \\ \left. - \frac{1}{\eta^2} w - \frac{2 \sin(\theta)}{\eta^2} \left( \frac{\partial v}{\partial \varphi} \right) \right\} \end{aligned} \quad (5)$$

$$\frac{\partial T}{\partial t} + u \frac{\partial T}{\partial r} + \frac{1}{r} v \frac{\partial T}{\partial \theta} + \frac{1}{\eta} w \frac{\partial T}{\partial \varphi} = \frac{1}{Re.Pr} \left[ \frac{1}{r} \frac{\partial T}{\partial r} + \frac{\cos(\theta)}{\eta} \frac{\partial T}{\partial r} + \frac{\partial^2 T}{\partial r^2} - \frac{\sin(\theta)}{r\eta} \frac{\partial T}{\partial \theta} + \frac{1}{r^2} \frac{\partial^2 T}{\partial \theta^2} + \frac{1}{\eta^2} \frac{\partial^2 T}{\partial \varphi^2} \right] \quad (6)$$

## Numerical Method

The projection algorithm is used to solve the governing equations. This algorithm was introduced by Chorin [17] for the first time. In this approach, finite difference forms of the continuity and momentum equations are obtained based on the forward difference in time and the central difference in space. The overview of the image of the projection algorithm is expressed by Eqs. 7-9.

$$\frac{\mathbf{V}^* - \mathbf{V}^n}{\Delta t} + (\mathbf{V}^n \cdot \nabla) \mathbf{V}^n = \frac{1}{Re} \nabla^2 \mathbf{V}^n \quad (7)$$

$$\nabla^2 p^{n+1} = \frac{\nabla \cdot \mathbf{V}^*}{\Delta t} \quad (8)$$

$$\frac{\mathbf{V}^{n+1} - \mathbf{V}^*}{\Delta t} + \nabla p^{n+1} = 0 \quad (9)$$

In this algorithm, momentum equations are split into Eqs. 7 and 9 via auxiliary velocity,  $\mathbf{V}^*$ . The Poisson equation, Eq. 8, is obtained by means of taking the divergence of Eq. 9. According to the projection algorithm, first initial velocity field,  $\mathbf{V}^n$  is guessed and auxiliary velocity field,  $\mathbf{V}^*$ , is determined via Eq. 7. To obtain pressure field, the auxiliary velocity is substituted into Eq. 8 and line by line method is used to solve the system of the equations. Finally, the velocity field is corrected by Eq. 9. As this flow is steady-state, transition terms have to be disappeared at the steady state solution. So, the convergence of the code is assumed by:

$$\text{Max} \left\{ \left| \frac{\partial u}{\partial t} \right|, \left| \frac{\partial v}{\partial t} \right|, \left| \frac{\partial w}{\partial t} \right| \right\} \leq 10^{-6} \quad (10)$$

## Boundary Conditions

The inlet and outlet velocity conditions are considered to be uniform and fully developed respectively.

$$\begin{aligned} \text{At } \varphi = 0: \quad & u = v = 0, \quad w = 1 \\ \text{At } \varphi = \frac{3\pi}{2}: \quad & \frac{\partial u}{\partial \varphi} = \frac{\partial v}{\partial \varphi} = \frac{\partial w}{\partial \varphi} = 0 \end{aligned} \quad (11)$$

The length of the curved pipe is assumed to be long enough so that for 270-degree pipe and curvature ratio of 0.15, the flow can reach a fully-developed condition. No-slip condition is assumed at both inner and outer walls:

$$r = r_o, r = r_i: \quad u = v = w = 0 \quad (12)$$

Because of symmetry of the flow field with respect to the horizontal mid-plane, just the upper half of the cross section is simulated.

At the plane of symmetry:

$$\theta = 0, \theta = \pi: \frac{\partial u}{\partial \theta} = \frac{\partial w}{\partial \theta} = 0 \quad v = 0 \quad (13)$$

The thermal boundary conditions used for this issue are the ambient temperature at the inlet, insulation at the outer wall, symmetry in the  $\theta$  direction on the mid-plan and non-uniform heat source at the solid core. In the  $\varphi$  direction, the conduction heat transfer is negligible compared to forced convection so the outlet boundary condition in the  $\varphi$  direction doesn't pose any problem in the numerical scheme.

$$\begin{aligned} \varphi = 0: \quad T &= 0 \\ \theta = 0, \pi: \quad \frac{\partial T}{\partial \theta} &= 0 \\ r = r_o: \quad \frac{\partial T}{\partial r} &= 0 \\ r = r_i: \quad q'' &= B e^{A\theta} \end{aligned} \quad (14)$$

### Grid Independency Test and Code Validation

In order to verify grid independency of the numerical results, calculations are made for three different meshes of 30\*10\*20, 70\*45\*50 and 100\*55\*75 in the  $\varphi, r, \theta$  direction. Fig. 2 Shows changes of axial velocity on the symmetry plane based on different meshes. It is obvious from Fig. 2 that there is no significant difference between solutions based on the two last meshes, so the second mesh is chosen for further calculations. The flow behaviour through both the curved pipe with very low curvature ratio and the straight pipe is expected to be the same. Fig. 3 indicates a good correspondence between the axial flow velocity through the curved pipe with the curvature ratio of 0.001 and the analytical solution of the straight one. The axial velocity distribution of the annular flow is analytically obtained by White [18] as:

$$\frac{w}{w_{avg}} = \frac{-2}{r_o^2 + r_i^2 - \frac{r_o^2 - r_i^2}{\ln\left(\frac{r_o}{r_i}\right)}} \left[ (r^2 - r_i^2) - \frac{r_o^2 - r_i^2}{\ln\left(\frac{r_o}{r_i}\right)} \ln\left(\frac{r}{r_i}\right) \right] \quad (15)$$

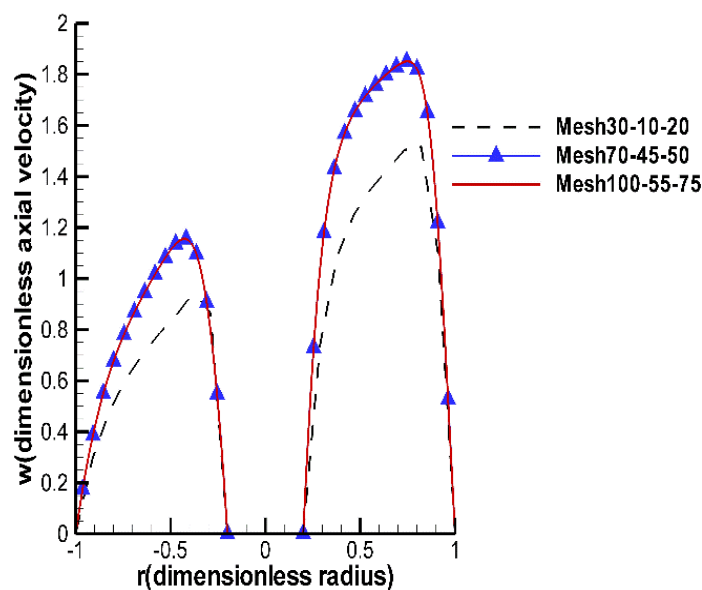


**Fig. 2.** Grid independency test on the three different meshes of 30\*10\*20, 70\*45\*50 and 100\*55\*75 (for curvature ratio of 0.15 and aspect ratio of 0.2)

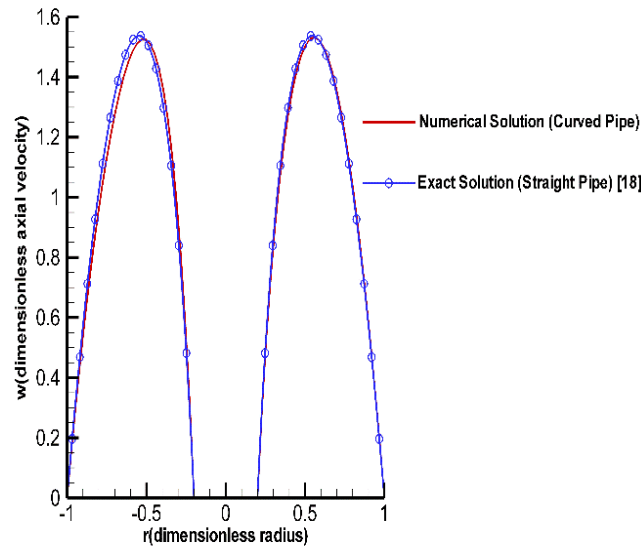


**Fig. 3.** Comparison between dimensionless axial velocity on the mid-plane of a curved pipe with a curvature ratio value of 0.001 and an analytical solution for similar straight pipe

## Results and Discussions

In the curved pipes, the centrifugal and pressure forces in the radius curvature direction cause to form a complicated flow field. An interaction between viscous, inertia, centrifugal and pressure forces provide a secondary flow in addition to the main flow. In Fig. 4, the secondary flow streamlines are shown in different cross section at  $Re=50$ . As seen in Fig. 4, two Dean vortices are formed so that the larger one is near the outer wall and the smaller one near the solid core. At  $Re=50$ , the center of the large vortex is in zone 1 because at low Reynolds number (here lower than 110) the viscous force dominates centrifugal force, besides the maximum effect of the centrifugal force which is imposed near the mid-plane in zone 1, is gradually transferred to upper parts of the zone 1. This is why that at low Reynolds number the maximum axial velocity is always in zone 1 (Fig. 5). At higher Reynolds number, the flow field changes and the larger vortex split into two smaller vortices (Fig. 6 for  $Re=500$ ). As Reynolds number increases, centrifugal force dominates the flow field and high momentum fluid particles (far away from the walls) move out from zone 1 to zone 2. So, the location of maximum axial velocity moves from the inner part to the outer part as shown in Fig. 7.

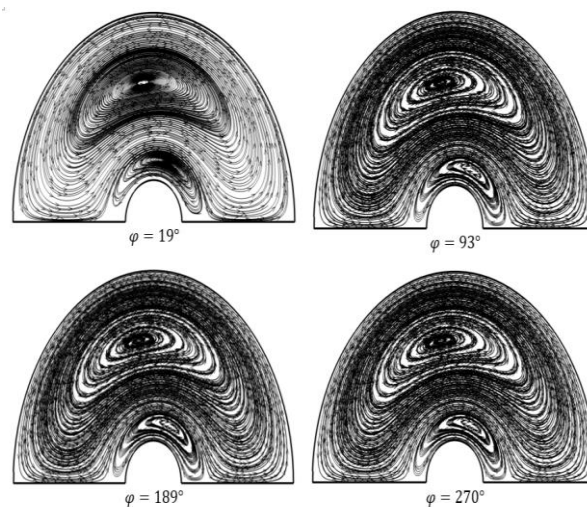


**Fig. 4.** Secondary flow streamline at different cross sections (for  $Re=50$ , curvature ratio: 0.15 and aspect ratio: 0.2)

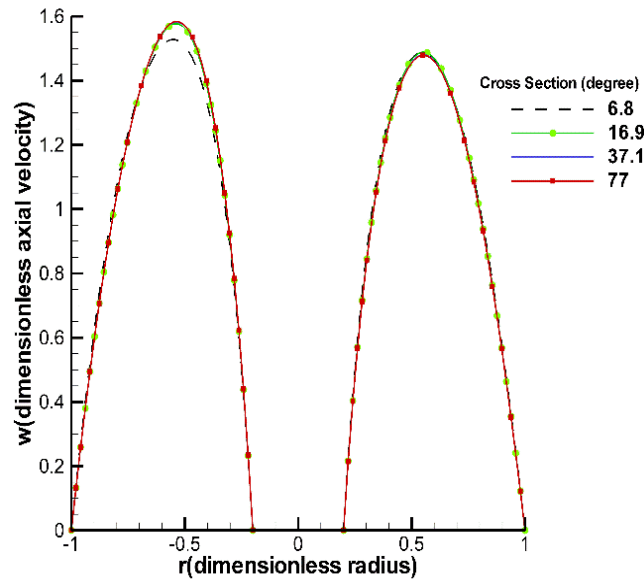


**Fig. 5.** Dimensionless axial velocity versus dimensionless radius on the mid-plane (for  $Re=50$ , curvature ratio: 0.15 and aspect ratio: 0.2)

One of the increasing heat transfer method through the curved pipe is the use of a non-uniform heat source rather than a uniform one. Here, the non-uniform heat flux is considered as  $q'' = Be^{A\theta}$ . As it is clear from this function, generated heat flux increases from zone 2 toward zone 1. Fig. 8 shows that the average Nusselt number is increased when non-uniform heat flux is used instead of the uniform one, i.e.  $A=0$ , assuming that all have the same average flux values.

Although according to this function, the amount of heat generation in zone 2 is less than zone 1, it is balanced by the higher axial velocity and forced convection heat transfer in zone 2. The effect of aspect ratio on the average Nusselt number is shown in Fig. 9. Due to a reduction in the aspect ratio, the centrifugal force dominates viscous force, therefore both axial velocity and forced convection heat transfer are increased. In the higher aspect ratio, in Fig. 9 for  $N=0.9$  and 0.5, there are no fluctuations for the average Nusselt number due to dominant viscous forces.

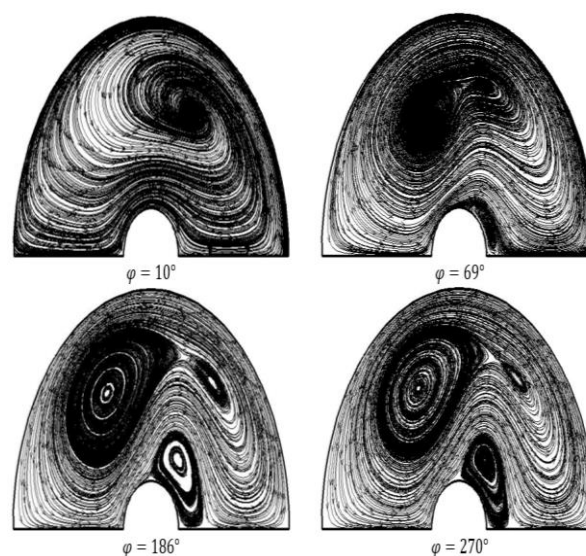


**Fig. 6.** Secondary flow streamline at different cross sections (for  $Re=500$ , curvature ratio: 0.15 and aspect ratio: 0.2)

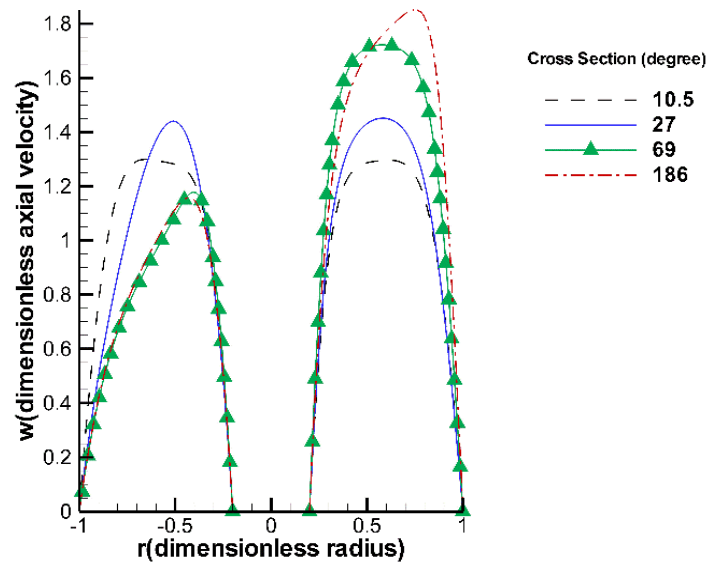


**Fig. 7.** Dimensionless axial velocity versus dimensionless radius on the mid-plane (for  $Re=500$ , curvature ratio: 0.15 and aspect ratio: 0.2)

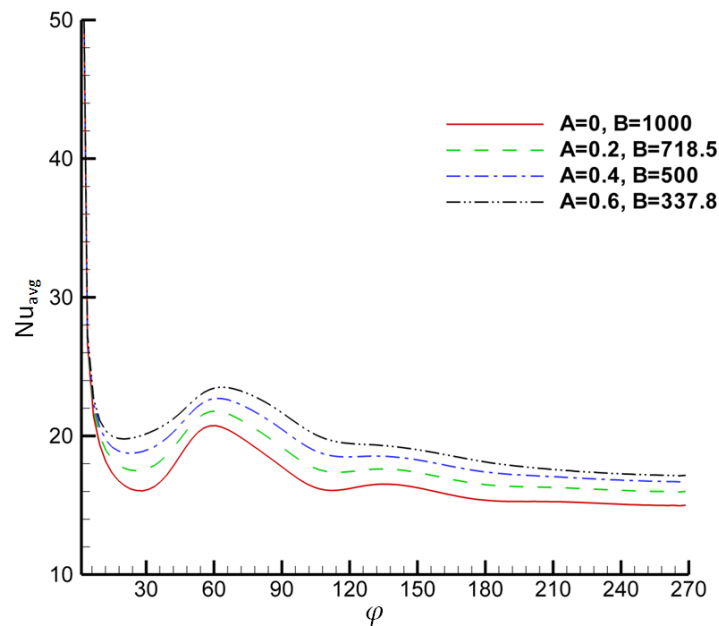


**Fig. 8.** The peripherally averaged Nusselt number along the wall of the solid core at the different coefficients of the heat source function, i.e.  $q''=Be^{A\theta}$ , (for  $Re=500$ , curvature ratio: 0.15 and aspect ratio: 0.2)

**Fig. 10** indicates the effect of Reynolds number on the peripherally averaged Nusselt number along the wall of the solid core at the aspect ratio of 0.2 and  $A=0$  (i.e. uniform heat source). It is obvious from **Fig. 10** that the circumferentially averaged Nusselt number increases while Reynolds numbers are increased. At high Reynolds numbers, an increase of centrifugal forces cause a fluctuation in the average Nusselt number, but at low Reynolds numbers because of the presence of dominant viscous forces, there are no fluctuations.

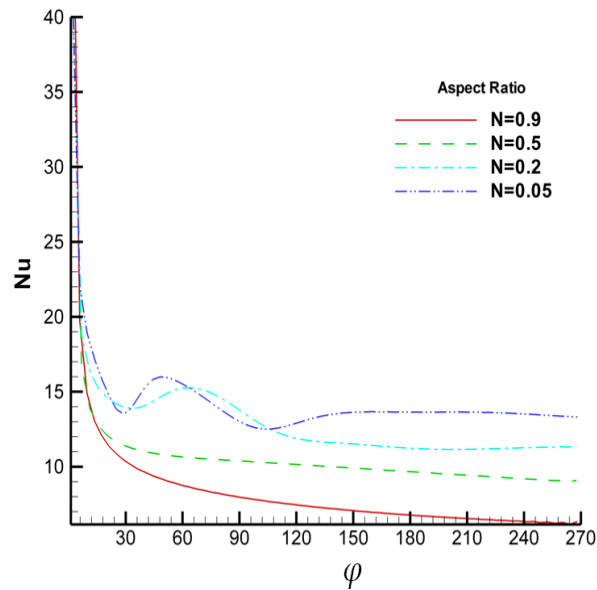


**Fig. 9.** The peripherally averaged Nusselt number along the wall of the solid core at the different aspect ratios (for non-uniform heat source on the core, i.e.  $q''=500e^{0.4\theta}$ ,  $Re=300$ , curvature ratio: 0.15 and aspect ratio: 0.2)

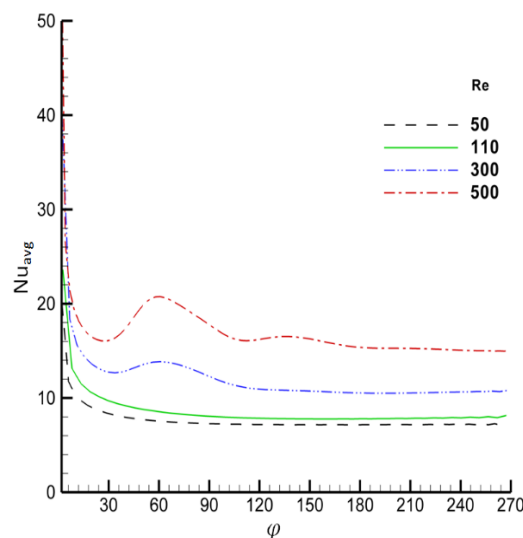


**Fig. 10.** The peripherally averaged Nusselt number along the wall of the solid core at the different Reynolds numbers (for uniform heat source on the core, i.e.  $q''=1000$ ,  $Re=500$ , curvature ratio: 0.15 and aspect ratio: 0.2)

## Conclusions

In this paper, thermo-hydraulic characteristics of annular flow through 270-degree curved pipe, including velocity field and average Nusselt number, are investigated. To simulate numerically this problem by the projection algorithm, the non-dimensional governing equations of continuity, full Navier-Stokes and energy equations are discretized based on the forward difference in time and the central difference in space. The results indicated that both the secondary flow field pattern and location of maximum axial velocity were changed at different Reynolds numbers. The effects of the non-uniform heat source compared with the uniform one and aspect ratio on heat transfer were studied. The numerical results showed heat transfer increases as the aspect ratios are decreased because of dominant centrifugal force in the flow field.

## Reference

- [1] Dean WR. XVI. Note on the motion of fluid in a curved pipe. *The London, Edinburgh, and Dublin Philosophical Magazine and Journal of Science*. 1927 Jul 1;4(20):208-23.
- [2] Robertson AM, Muller SJ. Flow of Oldroyd-B fluids in curved pipes of circular and annular cross-section. *International Journal of Non-Linear Mechanics*. 1996 Jan 1;31(1):1-20.
- [3] Kapur JN, Tyagi VP, Srivastava RC. Streamline flow through a curved annulus. *Applied Scientific Research, Section A*. 1965 Jan 1;14(1):253-67.
- [4] Hoon KC, Park SO. Laminar entrance flow in curved annular ducts. *International Journal of Heat and Fluid Flow*. 1992 Mar 1;13(1):41-9.
- [5] Petrakis MA, Karahalios GT. Steady flow in a curved pipe with a coaxial core. *International Journal for Numerical Methods in Fluids*. 1996 Jun 30;22(12):1231-7.
- [6] Petrakis MA, Karahalios GT, Kaplanis S. Steady flow in a curved pipe with circular cross-section. comparison of numerical and experimental results. *The Open Fuels & Energy Science Journal*. 2009 May 26;2(1):20-6.
- [7] Kara-halios GT. Mixed convection flow in a heated curved pipe with core. *Physics of Fluids A: Fluid Dynamics*. 1990 Dec;2(12):2164-75.
- [8] Park SM. Numerical simulation of core-annular flow in curved pipe [master's degree]. Delft: Delft University of Technology; 2014.
- [9] Guan X, Martonen TB. Simulations of flow in curved tubes. *Aerosol Science and Technology*. 1997 Jan 1;26(6):485-504.
- [10] Tarbell JM, Samuels MR. Momentum and heat transfer in helical coils. *The Chemical Engineering Journal*. 1973 Jan 1;5(2):117-27.
- [11] Pantokratoras A. Steady laminar flow in a 90 bend. *Advances in Mechanical Engineering*. 2016 Sep;8(9):1-9.
- [12] Riley N. Unsteady fully-developed flow in a curved pipe. *Journal of Engineering Mathematics*. 1998 Jul 1;34(1-2):131-41.
- [13] Hasan LD. Transient Three-dimensional Numerical Analysis of Forced Convection Flow and Heat Transfer in a Curved Pipe. *IOSE Journal of Mechanical and Civil Engineering*. 2013;9(5):47-57.
- [14] Dutta P, Nandi N. Effect of Reynolds number and curvature ratio on single phase turbulent flow in pipe bends. *Mechanics and Mechanical Engineering*. 2015;19(1):5-16.
- [15] Austin LR, Seader JD. Entry region for steady viscous flow in coiled circular pipes. *AIChE Journal*. 1974 Jul;20(4):820-2.
- [16] Siggers JH, Waters SL. Steady flows in pipes with finite curvature. *Physics of Fluids*. 2005 Jul 6;17(7):077102.
- [17] Chorin AJ. Numerical solution of the Navier-Stokes equations. *Mathematics of Computation*. 1968;22(104):745-62.
- [18] White FM, Corfield I. *Viscous fluid flow*. New York: McGraw-Hill; 2006.